

Lawrence Berkeley National Laboratory

Recent Work

Title

MICROSTRUCTURE-PROPERTY RELATIONSHIPS OF RARE EARTH-ZINC OXIDE VARISTORS

Permalink

<https://escholarship.org/uc/item/7w45k6bj>

Author

Williams, P.

Publication Date

1979-11-01

00105902414

UC-25
LBL-9805 e.1
Preprint

130



Lawrence Berkeley Laboratory

UNIVERSITY OF CALIFORNIA

Materials & Molecular Research Division

Submitted to the Journal of Applied Physics

MICROSTRUCTURE-PROPERTY RELATIONSHIPS
OF RARE EARTH-ZINC OXIDE VARISTORS

RECEIVED
LAWRENCE
BERKELEY LABORATORY

P. Williams, O. L. Krivanek, M. Yodogawa,
and G. Thomas

FEB 21 1980

LIBRARY AND
DOCUMENTS SECTION

November 1979

For Reference
Not to be taken from this room



Prepared for the National Science Foundation under Contract
DMR 77-24022 and the U. S. Department of Energy under Contract
W-7405-ENG-48.

LBL-9805-e.1

DISCLAIMER

This document was prepared as an account of work sponsored by the United States Government. While this document is believed to contain correct information, neither the United States Government nor any agency thereof, nor the Regents of the University of California, nor any of their employees, makes any warranty, express or implied, or assumes any legal responsibility for the accuracy, completeness, or usefulness of any information, apparatus, product, or process disclosed, or represents that its use would not infringe privately owned rights. Reference herein to any specific commercial product, process, or service by its trade name, trademark, manufacturer, or otherwise, does not necessarily constitute or imply its endorsement, recommendation, or favoring by the United States Government or any agency thereof, or the Regents of the University of California. The views and opinions of authors expressed herein do not necessarily state or reflect those of the United States Government or any agency thereof or the Regents of the University of California.

MICROSTRUCTURE-PROPERTY RELATIONSHIPS
OF RARE EARTH-ZINC OXIDE VARISTORSP. Williams*, O.L. Krivanek*, M. Yodogawa[†], and G. Thomas*

*Department of Materials Science and Mineral Engineering
Materials and Molecular Research Division
Lawrence Berkeley Laboratory
University of California, Berkeley, CA 94720 USA

[†]Ceramics Research Division
TDK Electronics
2-15-7 Higashiohoda
Ichikawa-shi
Chiba 272-01, Japan

ABSTRACT

The microstructure and properties of ZnO varistors containing Ba, Co, and rare earth metal oxides, which give values of α ($\alpha = d(\log I)/d(\log V)$) as high as 29, are examined. Mean ZnO grain size is $11\mu\text{m}$, and the grains are uniformly doped with Co. The barium and rare earth metals concentrate into $1.5\mu\text{m}$ wide particles embedded in a matrix of the ZnO grains. Within the grains and at grain boundaries, the barium and rare earth metal concentration is below the detection limit of the EDS technique (about 0.5%). No intergranular films, amorphous or crystalline, are detected, to within 10\AA resolution. These results are shown to be consistent with the grain boundary charge depletion model for the voltage barrier formation and breakdown.

I. INTRODUCTION

The zinc oxide varistor is a polycrystalline ceramic which exhibits rapidly increasing electrical conductivity with increased applied voltage. (1-5) The primary constituent is zinc oxide, usually 95 mole percent or more. In addition to the zinc oxide, the varistor contains smaller amounts of various other metal oxide constituents, such as Al_2O_3 , Bi_2O_3 , CoO , Co_3O_4 ,

Cr_2O_3 , MgO , MnO , NiO , Sb_2O_3 , SiO_2 , Sn_2O_3 , TiO_2 , Pr_2O_3 , and La_2O_3 .

The electrical properties of varistors are usually described by the nonlinear coefficient α , which is defined as $\alpha = d(\log I)/d(\log V)$ (i.e., $I = cV^\alpha$), where I is the current through the varistor, V is the applied voltage, and c is a constant. Commercial varistors have maximum α values in the range of 30-50; these values depend on which metal oxides are added to the basic zinc oxide and the sintering conditions.⁽²⁾ A consensus exists that the increase in conductivity is due to break-down of voltage barriers at grain boundaries,⁽²⁻¹⁵⁾ but the mechanism of the breakdown is explained either as electron tunneling through an insulating amorphous metal oxide phase separating the ZnO grains,⁽¹⁻⁴⁾ or by breakdown of charge depletion layers^(6,7) within ZnO grain regions adjacent to grain boundaries and/or intergranular oxide layers.⁽⁵⁾

The presence of continuous insulating oxide films at all, or at least most, grain boundaries, or the presence of doping profiles at grain boundaries, are of crucial importance in confirming either hypothesis. Early electron microscopical observations on ZnO varistors with Bi_2O_3 , CoO , MnO , Cr_2O_3 , and Sb_2O_3 tended to confirm the presence of the grain boundary films,⁽¹⁻⁵⁾ while in more recent studies, second phases were found located only⁽¹²⁾ or mostly^(13,14,15) at grain boundary junctions. An Auger study of grain boundaries exposed by fracture in a Bi-doped varistor⁽¹²⁾ has revealed a 20Å wide Bi-enriched layer. Two X-ray microanalysis studies^(14,16) of a similar varistor in scanning transmission electron microscopes have also found Bi enrichment at grain boundaries, including boundaries free of separate intergranular phases.⁽¹⁵⁾ Here, we report on a microstructural and microchemical characterization of varistors manufactured by TDK Electronics, and we correlate the observed microstructures with the varistors' electrical properties.

II. EXPERIMENTAL

Three ZnO varistor samples, all with 10 mole% CoO, .8 mole% BaO, .2 mole% NdO, and .25% Sm₂O₃, but with different sintering treatment, were examined. Figure 1 shows the bulk specimen current-voltage characteristics, measured separately for the pre-breakdown and the breakdown regions. Values of α , the nonlinear coefficient, range from one at 5 volts/mm to 28 or 29 at 200 volts/mm.

Figure 2 shows scanning electron micrographs of the three samples, taken at the same magnification. These micrographs show two phases: straight-sided zinc oxide grains and small particles, located at grain boundaries and within the grains. The microstructures of the three samples are quite similar, except that Sample 1 has the smallest mean zinc oxide grain size, while Sample 3 has the lowest population of particles. The mean zinc oxide grain sizes are 9.8 ± 1.3 microns, 11.7 ± 1.9 microns, and 12.1 ± 1.5 microns for Samples 1, 2, and 3, respectively. For all three samples, the mean particle width is 1.5 ± 0.7 microns, with larger but fewer particles at grain boundaries than within the grains.

Figure 3a is a higher magnification scanning electron micrograph of Sample 1, showing a ZnO grain (marked A) and a second phase particle (marked B). Figure 3b shows the results of X-ray compositional analysis conducted on these two areas in a scanning electron microscope (SEM) equipped with a Si(Li) energy-dispersive spectrometer (EDS). The grain contains zinc and cobalt, with a larger concentration of zinc than cobalt as indicated by the relative heights of their K α peaks. In contrast,

the particle contains zinc, cobalt, barium, neodymium, and samarium, with a larger concentration of zinc than of the other elements present except probably oxygen, which is not detectable by the EDS technique. Similar compositions were also found in Samples 2 and 3.

Imaging and analysis of ion-beam thinned samples in a transmission electron microscope equipped with a scanning attachment and EDS confirmed the SEM results. Figure 4a is a transmission electron micrograph showing a ZnO grain (upper right), a grain boundary (upper left), and a second phase particle (lower left). EDS analysis was conducted on points a through g with about 200Å spatial resolution. The results were converted into cation atomic percentages using the k-factor procedure.⁽¹⁷⁾ Figure 4b shows these percentages plotted for the various points; a, c, d, and e fall within the ZnO grain, b is on the grain boundary, g is at the grain-second phase particle interface, and f falls within the particle. In the middle of the grains, the zinc and cobalt contents are, respectively, 87 and 13 percent. At the grain boundary, the composition is the same to within one percent. No barium, neodymium or samarium were detected within ZnO grains or at grain boundaries in concentrations greater than 0.5 atomic percent (the minimum detectable level of the EDS technique). At the zinc oxide-particle interface, the zinc content drops from 88 to 69 percent, with the largest change occurring within 0.5 micron of the interface, while the cobalt content changes very little. The particle composition was 47 to 54 percent zinc, 16 to 19 percent cobalt, 13 to 16 percent barium, 11 to 12 percent samarium, and 5 to 6 percent neodymium, and it varied from particle to particle. The absolute accuracy of these results is only about 50%, but the error is the same to within a few percent for all the different areas examined, and so comparisons can be made to much higher precision.

Analysis of selected area electron diffraction patterns of different orientations revealed the configuration of the unit cell for the two phases to be hexagonal. Figure 5 shows the 100 orientation electron diffraction patterns for the zinc-cobalt oxide phase and the zinc-other metals oxide phase. The c and a parameters were determined to be 5.20\AA and 3.25\AA for the zinc-cobalt oxide grains, and 9.99\AA and 6.22\AA for the zinc-other metal oxide particles, with slight changes from particle to particle.

Figure 6 shows bright field-dark field pairs of transmission electron micrographs of Sample 2. The top pair shows a three-grain junction and the bottom pair shows a two phase interface. All boundaries appear highly curved, and there is no indication of a discrete grain boundary phase, even though a phase as narrow as 20\AA would be detectable in the dark field micrographs as a bright line between two dark grains. (18)

Figure 7 shows a lattice fringe image transmission electron micrograph of a zinc-cobalt oxide grain boundary. Analysis of electron diffraction patterns indicated that for the grain on the right, the main diffracting atomic planes are 011 type, whose interplanar spacing is 2.5\AA . For the other grain, the main diffracting atomic planes are $2\bar{1}0$ type, whose interplanar spacing is 1.6\AA . The observed width of the boundary is about 5\AA , showing again that no intergranular phase much wider than 10\AA was present. The spacing of the fringes was measured as a function of the distance from the grain boundary to see if any change, related to

variation of composition,⁽¹⁹⁾ could be detected, but the result was negative. This was, however, not surprising, since the detection limit of this method is probably even worse than that of the EDS technique.

III. DISCUSSION

The three varistor samples have a microstructure consisting of two phases: zinc oxide grains uniformly doped with cobalt (evidenced by the minimal change in composition throughout the zinc oxide grain, as shown in Figure 4), and small particles composed of a zinc-other metals oxide solution (evidenced by the variation in composition and lattice parameters from particle to particle). The other metals are cobalt, barium, samarium, and neodymium, in order of decreasing concentration. Due to the high melting points of the rare earth metal oxides, it is unlikely that these were involved in liquid phase sintering. This is also confirmed by the fact that no intergranular glassy films could be detected.

The maximum α values of 28 or 29 for these varistors are comparable to those of the commercial GE-MOV varistor.^(3,4) The resistivity of the three samples is inversely proportional to the mean grain size, indicating that grain boundaries constitute voltage barriers, as confirmed by a voltage contrast SEM study of the same material.⁽¹⁰⁾

Grain boundaries were found to be free of continuous intergranular films both by dark field electron microscopy and by lattice imaging. This appears to rule out the insulating oxide model.⁽¹⁻⁴⁾ On the other hand, the lack of direct evidence for doping profiles at grain boundaries does not rule out the depletion layer model.^(6,7) This is because both the EDS and the lattice fringe spacing measurement techniques used here cannot

detect elements in much less than 0.5 percent concentration, while the electrical properties of the varistor grain boundaries will be influenced at much lower doping levels. Preliminary investigations by Auger spectroscopy of fracture-exposed grain boundaries have also yielded negative results,⁽²⁰⁾ but it is possible that some other spectroscopical technique with better sensitivity such as alpha-X microanalysis will prove more successful.

Furthermore, the current-voltage characteristics in the break-down region (Fig. 1) agree closely with the exponential relationship predicted by the depletion layer model. Even more powerful evidence for this model has recently been obtained by van Kemenade and Eijthoven,⁽¹¹⁾ who observed that direct injection of electrons into the grain boundary region of the varistors leads to a dramatic increase in the current between the two adjacent grains. This shows very directly that the voltage barrier was due to a depletion layer.

V. CONCLUSIONS

The varistor samples examined here have good nonohmic properties with α values of 29 or more, even though they do not contain the usual Bi_2O_3 . Samples with smaller mean grain size and larger particle populations have higher resistivity and breakdown voltages; this indicates that grain boundaries and two-phase boundaries act as barriers to conduction. These barriers are not due to thin insulating continuous oxide films at grain boundaries, since no such films were detected. The grain boundary charge depletion layer model for the varistor's nonohmic behavior, on the other hand, shows good agreement with the varistor bulk electrical characteristics, and is consistent with the EDS results.

ACKNOWLEDGEMENTS

The assistance of Dr. R. Geiss in the compositional analysis conducted on the Philips 301 microscope is gratefully acknowledged. The U.S. Department of Energy through the Materials and Molecular Research Division of the Lawrence Berkeley Laboratory and NSF (Contract #DMR 77-24022) provided research facilities, technical staff, and financial support. This work was also prepared with the support of the U. S. Department of Energy under Contract W-7405-ENG-48.

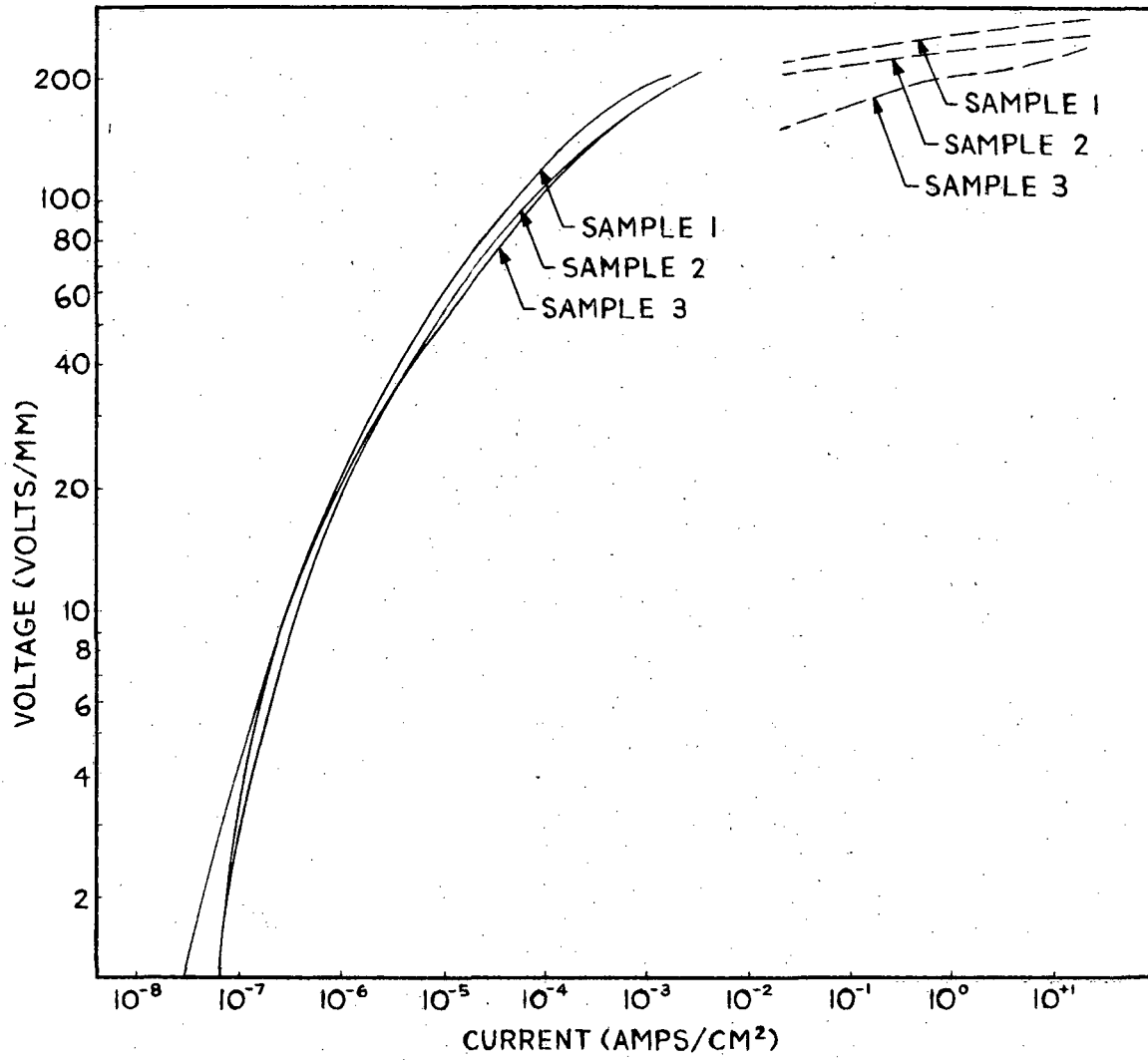
REFERENCES

1. M. Matsuoka, T. Masuyama, and Y. Iida, J. Jpn. Soc. Appl. Phys. Suppl. 39, 94 (1970).
2. M. Matsuoka, Jap. J. Appl. Phys. 10, 736 (1971).
3. Lionel M. Levinson and H.R. Philipp, G.E. Report #77-CRD110 (1977).
4. Lionel M. Levinson and H.R. Philipp, J. Appl. Phys. 46, 1332 (1975).
5. Kazuo Mukae, Koruchi Tsuda and Ikuo Nagasawa, Japan. J. Appl. Phys., 16, 1361 (1977).
6. W.G. Morris, J. Vac. Sci. Technol. 13, 926 (1976).
7. P.R. Emtage, J. Appl. Phys. 48, 4372 (1977).
8. R. Einzinger, Ber. Dtsch. Keram. Ges. 52, 244 (1975).
9. Joe Wong, J. Appl. Phys. 47, 4971 (1976).
10. O.L. Krivanek, P. Williams and Yi-Ching Lin, Appl. Phys. Lett. 34, 805 (1979).
11. J.T.C. van Kemenade and R.K. Eijnhoven, J. Appl. Phys. 50, 938 (1979).
12. W.G. Morris and J.W. Cahn, Grain Boundaries in Engineering Materials (Baton Rouge, LA: Claitors, 1975). William G. Morris, J. Vac. Sci. Tech., 13, 926 (1976).
13. D.R. Clarke, J. Appl. Phys., 49, 2407 (1978).
14. D.R. Clarke, Norelco Reporter, 26, 18 (1979).
15. A.T. Santhanam, T.K. Gupta, and W.G. Carlson, J. Appl. Phys. 50, 852 (1979).
16. W.D. Kingery, J.D. Vander Sande, and T. Mitamura, J. Am. Cer. Soc. 62, 221 (1979).
17. J.I. Goldstein, J.L. Costley, G.W. Lorimer and S.J.B. Reed, S.E.M. Proceedings 1, 315 (1977).

18. O.L. Krivanek, T.M. Shaw and G. Thomas, J. Appl. Phys. 50, 4223 (1979).
19. R. Sinclair, R. Gronsky and G. Thomas, Acta Met. 24, 789 (1976).
20. O.L. Krivanek, G. Todd and P. Williams, unpublished (1979).

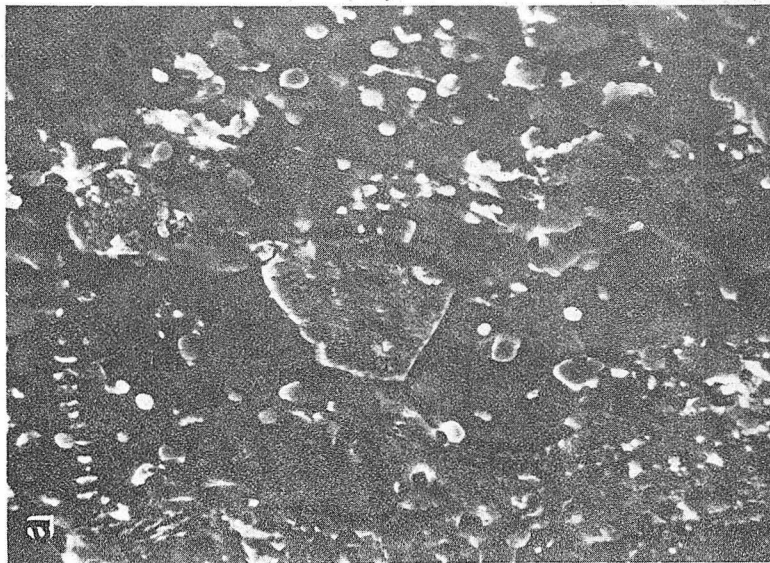
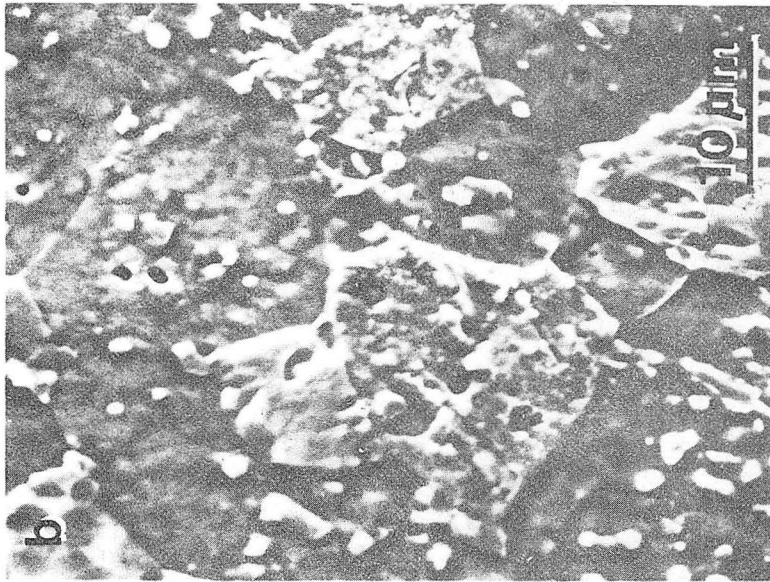
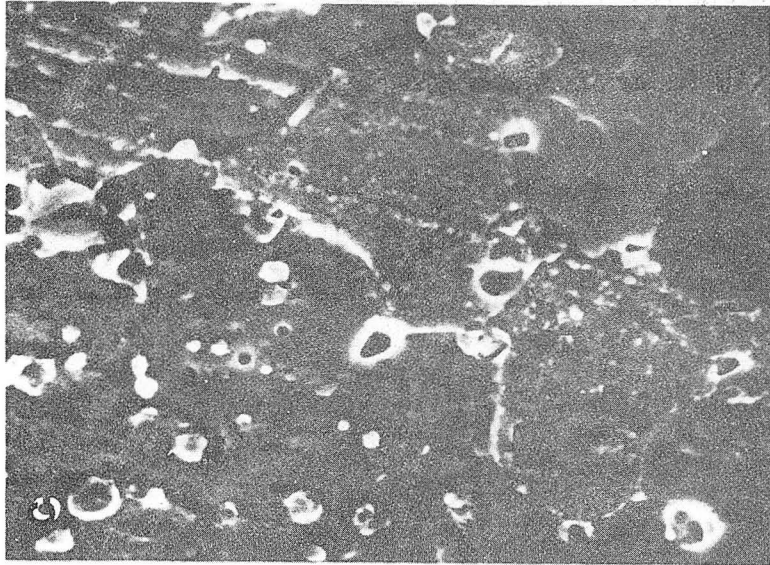
FIGURE CAPTIONS

- Fig. 1 V-I curves for the three varistors studied. The low and high current data were measured in separate experiments.
- Fig. 2 Scanning electron micrographs of Sample 1(a), Sample 2(b), and Sample 3(c).
- Fig. 3 A scanning electron micrograph of Sample 1(a), and the results of EDS analysis on a ZnO grain and a second phase particle (b).
- Fig. 4 A transmission electron micrograph of Sample 2(a) and the results of EDS analysis (b).
- Fig. 5 [100] electron diffraction patterns from a ZnO grain (a) and a second phase particle (b).
- Fig. 6 Bright field-dark field micrographs of a three-grain junction (top), and grain-particle (P) interface (bottom).
- Fig. 7 Lattice image of a ZnO grain boundary. Tilted illumination was used in a 3-beam condition.



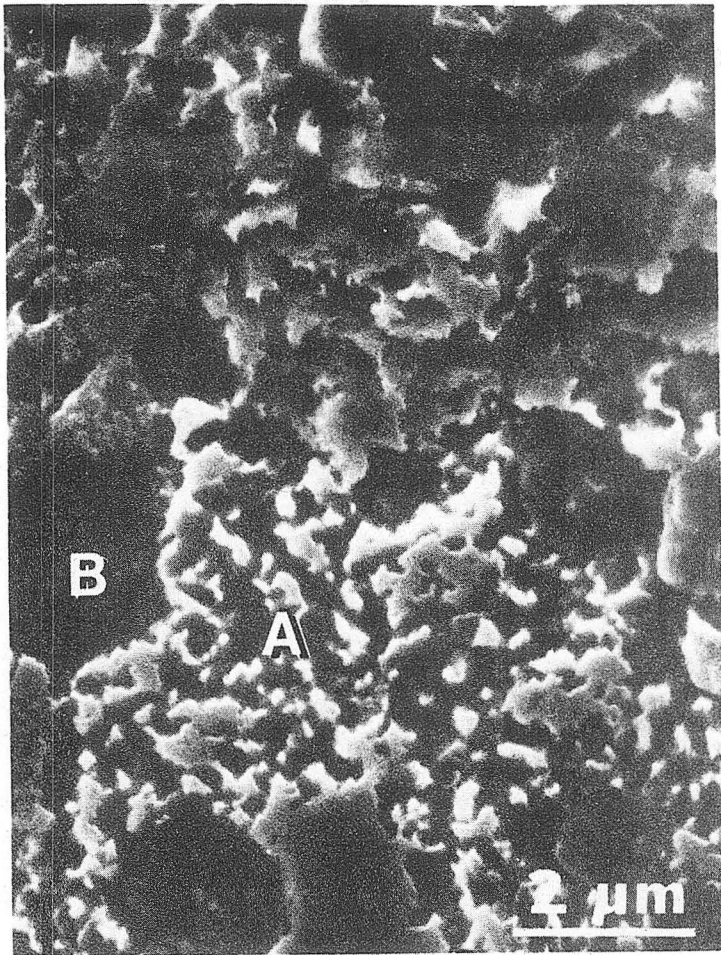
XBL 7910-12087

Fig. 1



XBB 799-12771

Fig. 2



(a)

(b)

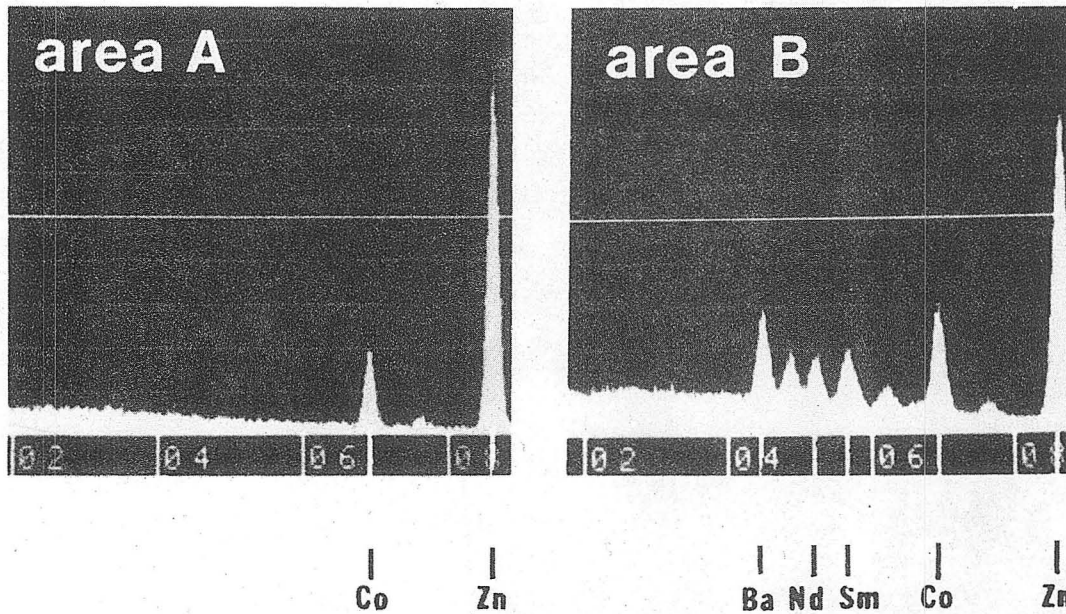
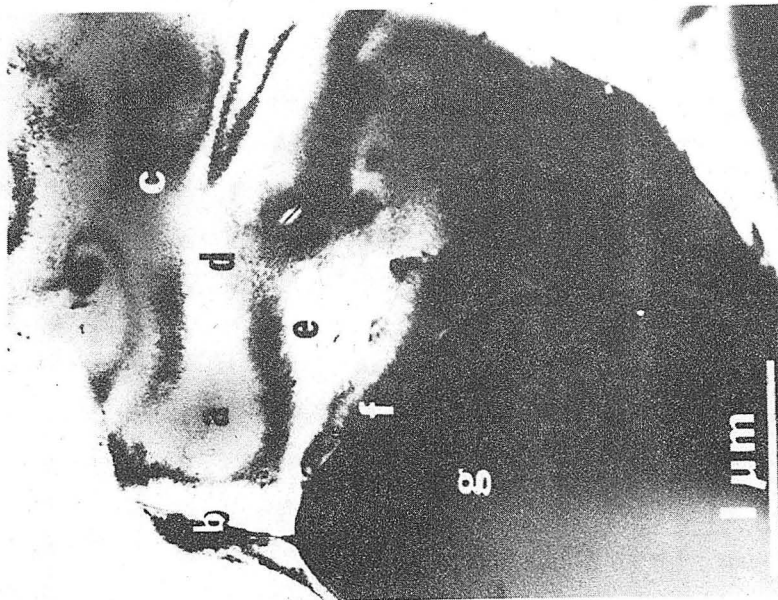


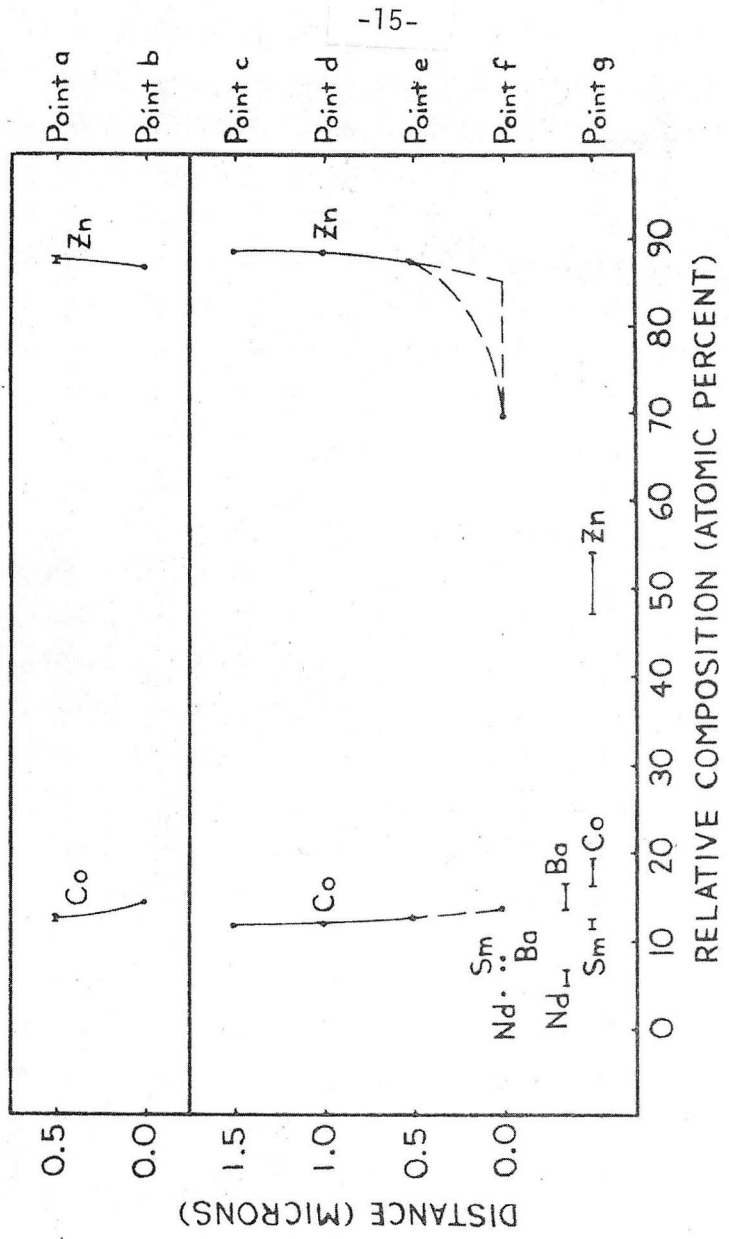
Fig. 3

XBB 799-12767

(a)

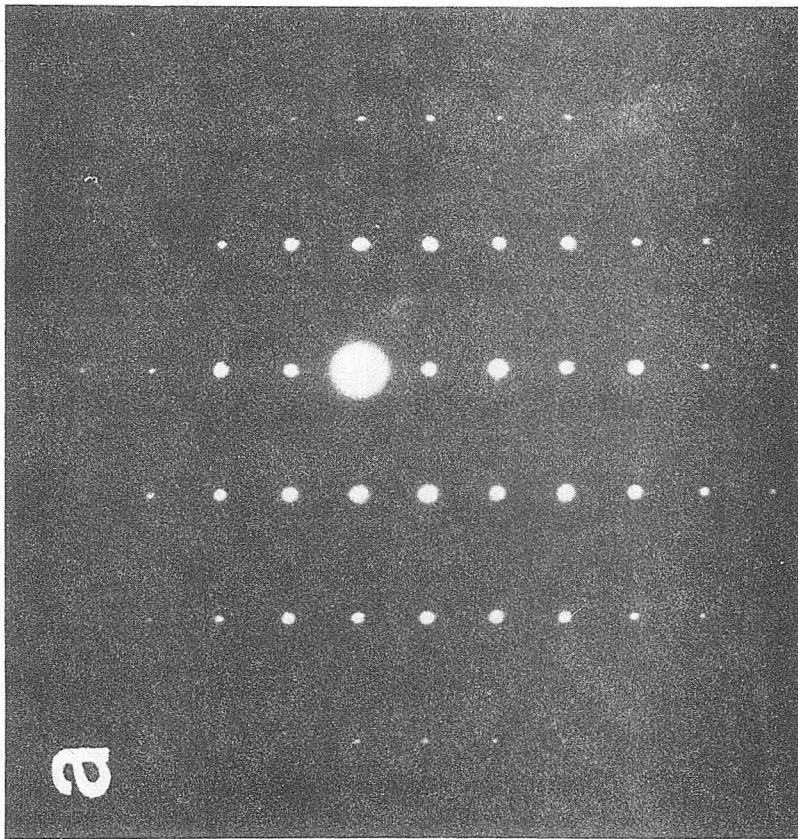
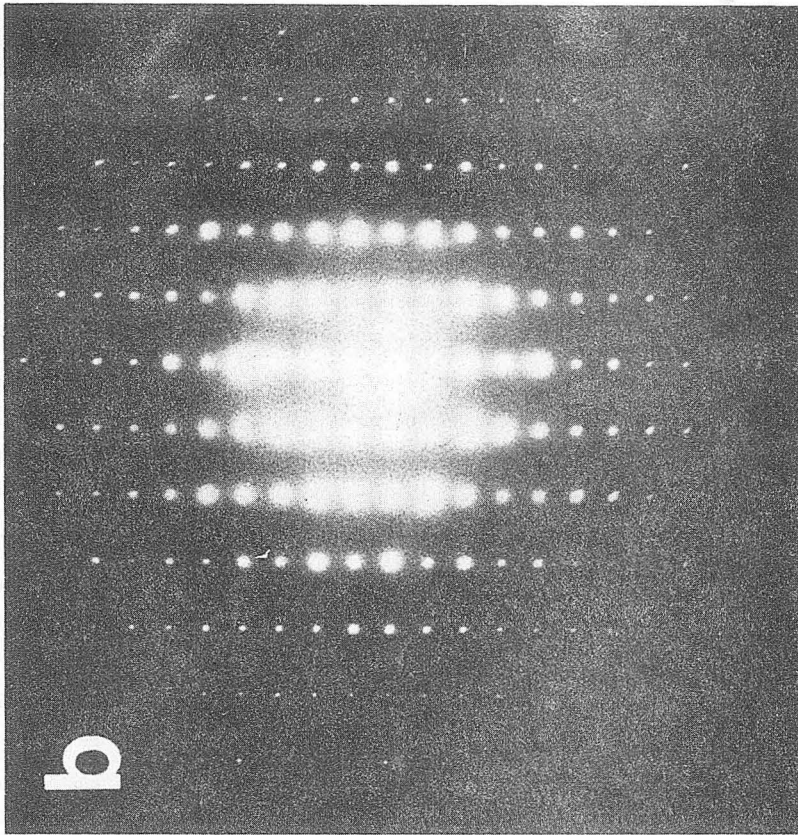


(b)



XBB 799-12766

Fig. 4



XBB 799-12768

Fig. 5

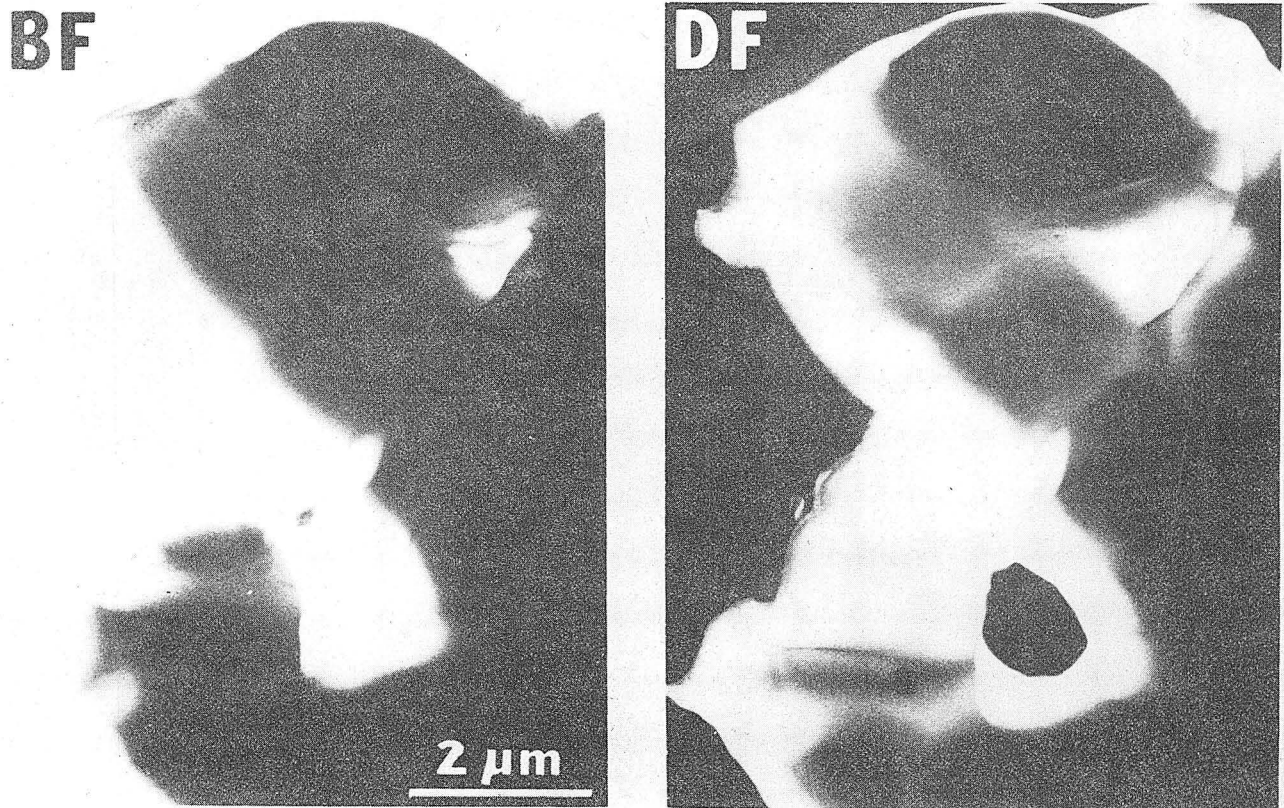
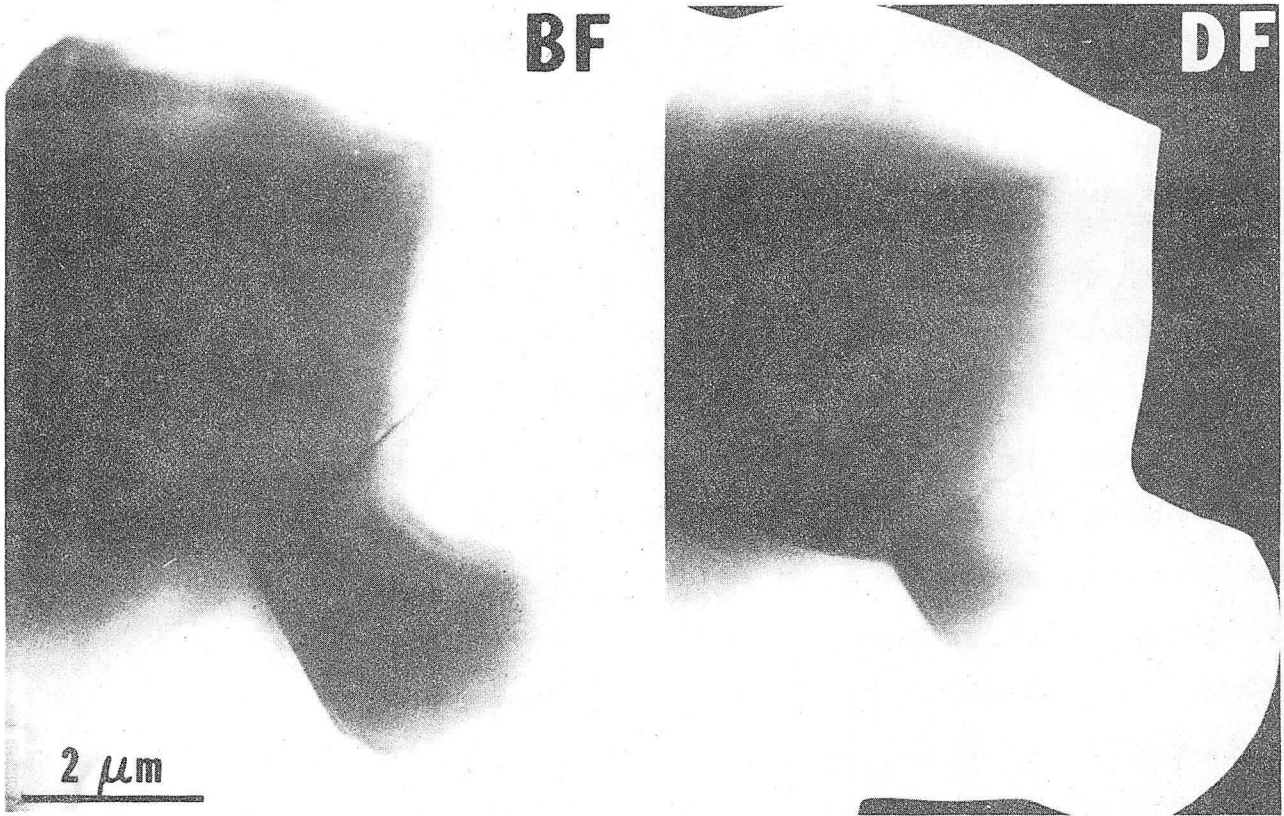


Fig. 6

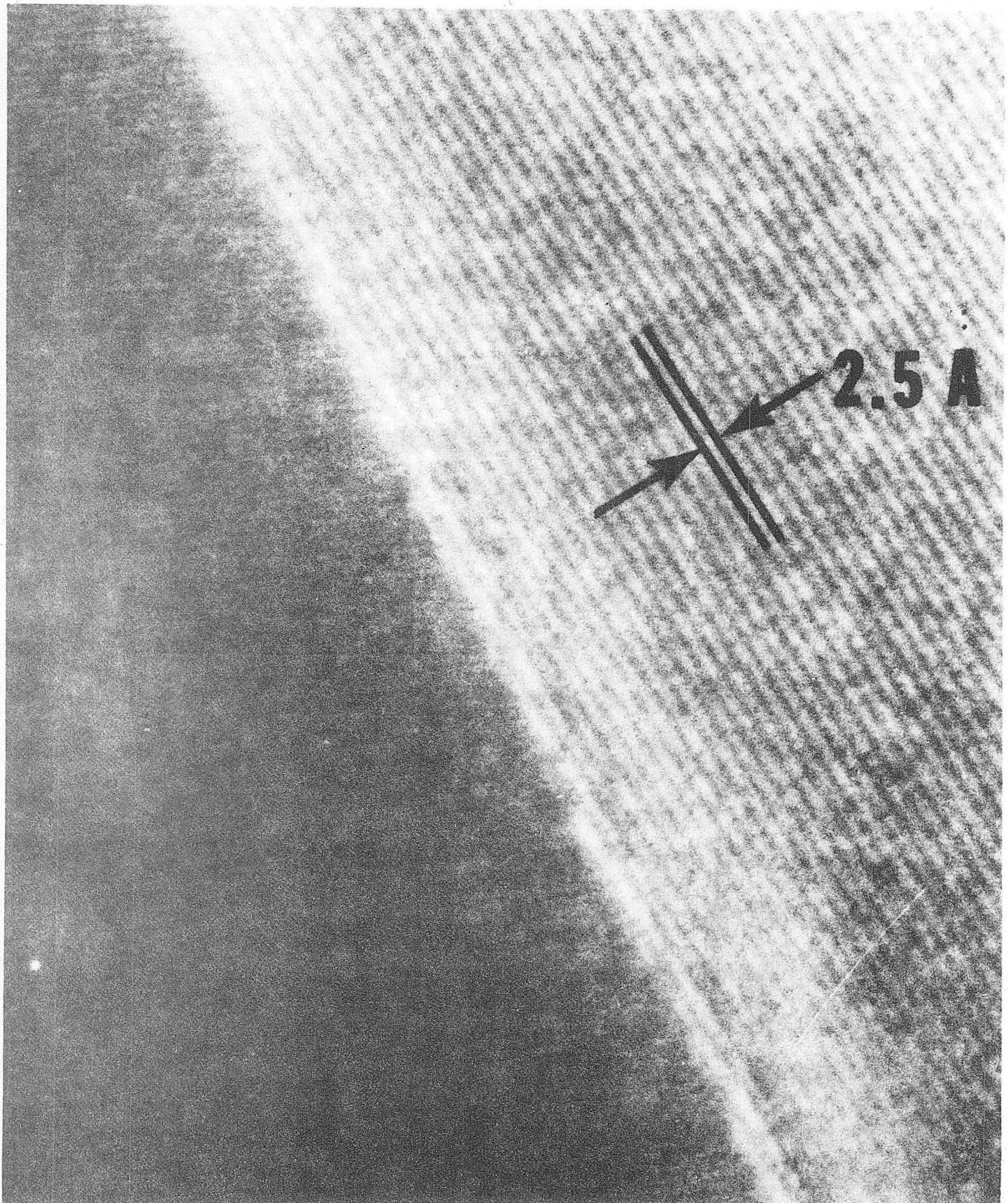


Fig. 7

XBB 799-12769

This report was done with support from the Department of Energy. Any conclusions or opinions expressed in this report represent solely those of the author(s) and not necessarily those of The Regents of the University of California, the Lawrence Berkeley Laboratory or the Department of Energy.

Reference to a company or product name does not imply approval or recommendation of the product by the University of California or the U.S. Department of Energy to the exclusion of others that may be suitable.

TECHNICAL INFORMATION DEPARTMENT
LAWRENCE BERKELEY LABORATORY
UNIVERSITY OF CALIFORNIA
BERKELEY, CALIFORNIA 94720